RSC Advances

PAPER

View Article Online
View Journal | View Issue

Cite this: *RSC Adv.*, 2025, **15**, 377

Sustainable superhydrophobic lignin-based polyurethane foam: an innovative solution for oil pollutant adsorption†

Xinglin Li,[a] Jing Zhang,[a] Hong Liu,[b] Zhiyu Li, *[a] Guanfeng Zheng,[a] Ling Zhou[c] and Peng Fu *[a]

Green, efficient treatment of crude oil spills and oil pollutants is a global challenge, with adsorption technology favored for its efficiency and low environmental impact. The development of an environmentally friendly adsorbent with high hydrophobicity, excellent adsorption performance, and degradability is crucial to overcoming the limitations of petroleum-based adsorbents. Here, a lignin-based polyurethane foam (LPUF) with superhydrophobic and photothermal oil-absorbing properties was fabricated by incorporating octadecyltrimethoxysilane into the foam system. The modified foam showed a 151.4° water contact angle, as long-chain alkyl groups reduced surface energy, giving it superhydrophobicity. The foam adsorbent exhibited remarkable adsorption performance for a variety of organic solvents, achieving a maximum adsorption capacity of 20 g g^{-1} and an oil–water separation efficiency exceeding 97%. Due to its outstanding elastic recovery properties, the foam exhibited only a 1.5% reduction in adsorption capacity after 10 adsorption–desorption cycles, indicating its strong potential for repeated adsorption and recovery. Under 1 kW m^{-2} sunlight intensity, the surface temperature of the foam adsorbent rose to 79.7 °C within 350 seconds. The excellent photothermal conversion properties of the foam significantly reduced the viscosity of the surface crude oil, thereby increasing the adsorption rate. In addition, the modified foam adsorbent also demonstrated self-cleaning properties and could be completely degraded after 5 hours of treatment in an alkaline solution. The developed LPUF adsorbent exhibited superior hydrophobicity and oil–water separation capabilities, highlighting its potential for efficient oil pollutant removal, while also offering new avenues for the high-value utilization of renewable resources.

Received 15th October 2024
Accepted 7th December 2024

DOI: 10.1039/d4ra07384c

rsc.li/rsc-advances

1. Introduction

With the advancement of technology and the increase in production levels, the environmental pollution caused by oily wastewater has become increasingly severe.[1] Meanwhile, oil spill incidents, including those involving petroleum, occur frequently. In 2023 alone, approximately 2000 tons of oil leaked into the natural environment due to tanker accidents, causing irreversible damage to both the economy and the ecological environment.[2–6] Currently, common methods for removing oil and organic pollutants include *in situ* burning, dispersants, and biodegradation.[7–10] However, these methods are not only costly and often ineffective, but they also frequently lead to secondary environmental pollution.[11,12] In recent years, porous foam adsorbents have gained significant attention as a solution to oil spills and organic pollutant leakage.[13,14] Porous foam absorbents are not only easy to operate, energy-efficient, and highly effective, but they also do not cause secondary environmental pollution. Therefore, they are considered to be an effective and economically viable solution.[15,16]

Polyurethane is a multifunctional polymer material with a variety of application forms.[17–19] Polyurethane foam (PUF) has the advantages of low permeability, excellent mechanical properties, low density, and high absorption efficiency. PUF material is considered to be one of the most promising foam adsorbents for removing oily pollutants from water.[20–22] Mallakpour *et al.*[23] immersed commercial polyurethane in a mixed solution of activated carbon black and sodium alginate to develop a composite PUF that can be used for oil spill adsorption. The oil adsorption capacity of the foam is as high as 21 g g^{-1}, and it exhibits rapid adsorption ability. Hoang *et al.*[24] added treated coconut shell fiber to the polyurethane matrix to prepare a new adsorbent with high oil adsorption efficiency.

[a]College of Agricultural Engineering and Food Science, Shandong University of Technology, Zibo, 255000, China. E-mail: fupengsdut@163.com; tarimlizhiyu@hotmail.com

[b]Binzhou Inspection and Testing Center, Binzhou, 256600, China

[c]Modern Agricultural Engineering Key Laboratory at Universities of Education Department of Xinjiang Uygur Autonomous Region, School of Mechanical Electrification Engineering, Tarim University, Alaer 843300, China

† Electronic supplementary information (ESI) available. See DOI: https://doi.org/10.1039/d4ra07384c

The oil adsorption capacity of the foam can reach 15.2 g g^{-1}, and it has good reusability. Sittinun *et al.*[25] extracted cellulose fiber from water hyacinth and added it to PUF to prepare a foam adsorbent for oil absorption. The addition of fibers successfully increased the porosity of the foam, and the oil adsorption of the material was in the range of 3.91–12.49 g g^{-1}, which is better than the original PUF. However, cellulose biomass has strong hydrophilicity, and its addition greatly reduces the water contact angle of the foam, limiting the oil–water separation performance of the material. The adsorption of oil spills from water environments requires the adsorbent to have a high water contact angle, so the development of hydrophobic PUFs that can be used for oil–water separation remains a research focus.

Superhydrophobic materials are defined as materials with a surface contact angle greater than 150°, exhibiting extremely strong hydrophobicity and excellent oleophilicity.[26,27] These materials feature low surface energy and high surface roughness, enabling them to preferentially adsorb oil-based substances in water environments, while water forms spherical droplets on their surface and rolls off rapidly. Capillary action enables oil-based substances to rapidly penetrate and fill the material's porous structure, ensuring efficient adsorption and storage.[28,29] Due to the hydrophobic and oleophilic characteristics of superhydrophobic materials, they have been widely used in oil–water separation and oil spill treatment.[30] Zimmermann *et al.*[31] developed a porous PUF material modified with organosilane, which was successfully applied in oil spill adsorption. The silanized foam exhibited a water contact angle of 110.2° and an oil adsorption capacity of 40–74 times its own weight, demonstrating excellent hydrophobicity and selectivity for oil. Yuan *et al.*[32] incorporated hierarchical hollow SiO_2@MnO_2 cubes into PUF, enhancing its hydrophobicity and adsorption performance. The modified foam had a water contact angle of 124° and an oil adsorption capacity of 31.6 g g^{-1} for carbon tetrachloride, and it retained its hydrophobicity and elasticity even after ten cycles of oil–water separation. Sabouri *et al.*[15] loaded magnetic nanoparticles into commercial PUF materials and modified them with stearic acid to obtain a superhydrophobic foam with a water contact angle of 148°. This foam had an oil adsorption capacity of 31.9 g g^{-1} for light crude oil and was highly effective in removing oil pollutants from water. It is important to note that the raw materials for commercial PUF are derived from petrochemical products, and their extensive use generates harmful waste and accelerates the depletion of fossil resources.[33,34] Therefore, there is a need for green, clean materials to compensate for the limitations of petrochemical products. Biomass materials, which are derived from biological resources and produced through biological, chemical, and physical processes, have the potential to replace petroleum-based polyols in the production of polyurethane materials.[35,36]

Biomass primarily consists of starch, cellulose, lignin, and hemicellulose, among which lignin is a widely available macromolecular organic substance with abundant reserves. However, due to its complex structure and limited reactivity, lignin has proven challenging to utilize for high-value applications.[37–41] The various functional groups in lignin provide excellent reaction sites for isocyanates, and its random amorphous network structure helps to enhance the mechanical and thermal properties of polyurethane materials, improving the material's stability.[42–45] Ma *et al.*[46] prepared lignin-based polyols (LLP) through a one-pot method and blended them with carbon nanotubes to produce LPUF materials. The resulting foam exhibited a water contact angle of 139.4° and an oil contact angle of only 76.1°. Thanks to the photothermal effect of the carbon nanotubes, the foam showed excellent heavy oil adsorption capacity. Wu *et al*[47] added SiO_2 modified with perfluorodecyltrichlorosilane to LLP and synthesized a superhydrophobic LPUF *via* a one-step foaming method. This foam achieved a water contact angle of 151.3°, with an adsorption capacity of 18 g g^{-1} and an oil recovery rate of approximately 93% after 20 cycles of oil adsorption. Moreover, due to the fact that the ether bonds in lignin (mainly β-O-4 bonds) are easily broken through thermal treatment, chemical processing, physical treatment, or biodegradation,[48] LPUF is readily degradable at the end of its life cycle, thereby reducing its environmental impact.[49,50] However, many reported superhydrophobic LPUF adsorbents typically contain a low proportion of lignin, limiting the extent to which petroleum-based polyols can be replaced. Therefore, there is an urgent need to develop a superhydrophobic LPUF adsorbent with a high lignin content and excellent oil–water separation performance.

In this study, a superhydrophobic and degradable LPUF was prepared, which demonstrated high efficiency in adsorbing crude oil and organic pollutants. First, lignin was subjected to catalytic liquefaction to produce LLP, and then LPUF was synthesized using a one-step foaming method. Subsequently, octadecyltrimethoxysilane was applied to modify the foam, imparting superhydrophobicity. We systematically investigated the effects of lignin content and octadecyltrimethoxysilane concentration on the microstructure and material properties of LPUF. Finally, the adsorption performance of the modified foam for crude oil and various organic solvents was studied, and its cyclic adsorption capacity was verified. Additionally, the inherent photothermal conversion properties of lignin further enhanced the foam's photothermal performance. Under light irradiation, the foam's surface temperature increased due to photothermal conversion, reducing the viscosity of the crude oil and accelerating the adsorption process. LPUF was shown to be completely degradable in alkaline solutions, thus reducing environmental pollution. The development of this material demonstrates the potential for converting biomass resources into functional materials in the field of environmental remediation, offering new possibilities for the promotion of green technologies in the future.

2. Materials and methods

2.1. Materials

The enzymatic hydrolysis lignin extracted from corncob was supplied by Shandong Long Li Biotechnology Co., Ltd, and was used without further purification or chemical modification. Polyethylene glycol-400, glycerol, sodium hydroxide, anhydrous ethanol, methanol, cyclohexanol, and deuterated chloroform were purchased from Shanghai Aladdin Biochemical

Technology Co., Ltd, China. Anhydrous pyridine, *n*-hexane, *n*-octane, chromium acetylacetonate, 2-chloro-4,4,5,5-tetramethyl-1,3,2-dioxaphospholane, hexamethylene diisocyanate, octadecyltrimethoxysilane, *n*-hexadecane, and dibutyltin dilaurate were purchased from Shanghai Macklin Biochemical Technology Co., Ltd Benzene, sulfuric acid, tetrahydrofuran, dichloromethane, and Oil Red O were obtained from Sinopharm Chemical Reagent Co., Ltd, China.

2.2. Preparation of liquefied lignin polyols (LLP)

The liquefaction of lignin was carried out according to previously reported methods.[46] First, enzymatic hydrolysis lignin particles were ground using a high-speed grinder for 1 minute until they reached a powdered state. Then, 80 g of PEG-400 and 20 g of glycerol were mixed in a three-neck glass flask. According to the formula in Table S1,† concentrated sulfuric acid was added to the mixture, followed by the gradual addition of lignin while stirring. The liquefaction reaction was then carried out at 140 °C under nitrogen protection for 1 hour. After the reaction, the product was rapidly cooled to room temperature, and the pH was adjusted to neutral using an appropriate amount of sodium hydroxide solution. The product was placed in a vacuum oven for 2 hours to remove water, resulting in a dark brown lignin-based polyol (LLP). The resulting LLPs were named LLP15, LLP22.5, LLP30, and LLP37.5, respectively.

2.3. Preparation of lignin-based polyurethane foam (LPUF)

According to the values and formulation in Table S2,† LPUF was prepared using a simple one-step foaming method. The [NCO]/[OH] ratio in all systems was 1.0. First, 20 g of LLP was added to a beaker, followed by 0.2 g of dibutyltin dilaurate (DBTDL, catalyst) and 0.06 g of water (foaming agent). The mixture was stirred for 5 minutes, after which hexamethylene diisocyanate (HDI) was added and rapidly stirred at high speed for 30 seconds. The final mixture was quickly poured into a paper cup at room temperature, where it foamed to form LPUF. Due to its high viscosity, LLP37.5 was unsuitable for foam preparation. The resulting LPUF samples were named LPUF15, LPUF22.5, and LPUF30, respectively.

2.4. Preparation of superhydrophobic LPUF

A mixed solution of ethanol/deionized water (V : V = 1 : 1) was prepared, and after adding octadecyltrimethoxysilane (ODTMS), the solution was hydrolyzed at room temperature for 5 minutes to prepare ODTMS solutions with concentrations of 0.5%, 1%, 1.5%, and 2%. The LPUF samples were immersed in the ODTMS solutions and heated in a water bath at 60 °C for 30 minutes. Afterward, the LPUF was repeatedly washed with ethanol and dried in an oven at 115 °C to obtain superhydrophobic foams. The resulting foams were named LPUF-0.5, LPUF-1, LPUF-1.5, and LPUF-2 based on the ODTMS solution concentration.

2.5. Characterization

The quantitative 31P nuclear magnetic resonance (NMR) spectrum of LLP was obtained using methods proposed in previous studies. The 31P NMR spectrum was acquired at room temperature on a Bruker Avance III 400 MHz instrument. The sample was dissolved in a mixture 500 μL of anhydrous pyridine and deuterated chloroform (V/V = 1.6 : 1). 10 mg of cyclohexanol was added as an internal standard, and 100 μL of the relaxation reagent chromium acetylacetonate solution (5.6 mg mL^{-1}, dissolved in a mixture of anhydrous pyridine and deuterated chloroform, V/V = 1.6 : 1) was introduced. Finally, after thorough mixing, 70 μL of the phosphitylation reagent 2-chloro-4,4,5,5-tetramethyl-1,3,2-dioxaphospholane was added for derivatization, and the solution was transferred to a 5 mm NMR tube for subsequent NMR analysis. The viscosity of LLP was measured using a rotational rheometer. Prior to observing the sample structure using scanning electron microscopy (SEM), all samples were sputter-coated with a platinum layer less than 10 nm thick using an ion sputter coater. The surface morphology of the samples was captured using a SEM (Sirion 200, Hong Kong). Elemental distribution maps of the samples were obtained using energy dispersive spectroscopy (EDS) attached to the SEM. X-ray photoelectron spectroscopy (XPS) analysis was performed using an X-ray photoelectron spectrometer (Axis Ultra DLD, UK). Fourier-transform infrared (FTIR) spectra were recorded using a Nicolet iS50 spectrometer (USA), with all spectra collected at room temperature over a range of 400 to 4000 cm^{-1} and 32 scans per measurement. The water contact angle (WCA) was measured using an optical contact angle meter (OCA25, Germany), with 3 μL droplets as indicators. Thermogravimetric analysis (TGA) measurements were performed using a comprehensive thermogravimetric analyzer (SDT650, USA). All tests were conducted under a nitrogen atmosphere with a heating rate of 20°C min^{-1} from 50 to 800 °C. The cyclic compression tests were carried out using a universal testing machine at a compression speed of 50 mm min^{-1}. The foam samples were compressed along the growth direction to a strain of 75%, cycled 30 times. The sample dimensions were 30 mm × 30 mm.

2.6. Oil adsorption capacity experiment

The adsorption capacity of LPUF30-2 for various organic solvents with different densities (*n*-hexane, *n*-hexadecane, *n*-octane, toluene, benzene, tetrahydrofuran, dichloromethane) and crude oil was determined using a gravimetric method. LPUF30-2 was cut into 10 mm × 10 mm × 10 mm cubes and fully immersed in a beaker containing 30 mL of the oil substance for 5 minutes. The adsorption capacity was calculated by measuring the foam's mass before and after adsorption, using the following formula:

$$k = \frac{m_1 - m_0}{m_0} \quad (1)$$

In the formula, m_1 represents the weight of the sample after oil adsorption; $m_0$represents the weight of the sample before adsorption, and k is the adsorption capacity of the sample.

To test the reusability of the material, LPUF30-2 was fully immersed in an organic solvent or crude oil until saturation, followed by squeezing out the adsorbed oil completely. This adsorption-squeezing cycle was repeated 10 times, and the

adsorption capacity of the sample was recorded after each cycle. The oil–water separation performance of the foam adsorbent under gravity-driven conditions was evaluated using an oil–water separator. A mixture of 100 mL chloroform/water (V/V = 1 : 1, stained with Oil Red O and methylene blue, respectively) was poured into the filter cup. Under the influence of gravity, the chloroform passed through the superhydrophobic LPUF30-2 and into the receiving bottle, and the permeated liquid was collected. The oil–water separation efficiency was calculated using the following formula:

$$\eta = \frac{m_1}{m_0} \times 100\% \quad (2)$$

Due to the strong volatility of chloroform, the water was collected to calculate the oil–water separation efficiency. In the formula, m_0 represents the mass of the water before separation; m_1 represents the mass of the water after separation, and η is the oil–water separation efficiency of the sample.

2.7. Photothermal oil absorption experiment

Under simulated strong sunlight (1 kW m^{-2}) using a solar simulator (CEL-HXF300, China Education Au-Light Co., China), the infrared images and surface temperatures of LPUF30-2 and crude oil were measured using a thermal imaging camera (I50, FLIR, USA). The photothermal oil adsorption experiment was conducted as follows: First, crude oil was dropped onto the water surface, and then LPUF30-2 samples, cut into 15 mm × 15 mm × 10 mm dimensions, were placed on the water surface for the adsorption experiment. The entire adsorption process was recorded using both the thermal imaging camera and a regular camera.

2.8. Degradation and self-cleaning experiments

LPUF30-2 was cut into 5 mm × 5 mm × 10 mm pieces and placed in 20 mL of methanol-0.2 mol L^{-1} sodium hydroxide aqueous solution (V/V = 1 : 1). The sample vials containing the foam were subjected to degradation at 60 °C for 5 hours. The degradation efficiency was calculated using the following formula:

$$\text{Degradation efficiency}(\%) = \frac{\text{original weight} - \text{residual weight}}{\text{original weight}} \times 100\% \quad (3)$$

To simulate the self-cleaning property of the sample in a soil-contaminated environment, 0.3 g of soil particles were placed on top of LPUF30-2. Water droplets were then dropped onto the surface of the superhydrophobic LPUF30-2 foam, and the droplets gradually slid off the surface. The self-cleaning performance of the sample was evaluated based on this process.

3. Results and discussion

3.1. Superhydrophobic LPUF adsorbent

Lignin, as the main component of wood, possesses advantages such as being environmentally friendly, abundant, and renewable. [51] However, its complex aromatic structure and significant steric hindrance effects limit its direct application in polyurethane synthesis. [52] Therefore, we first liquefied the lignin. The preparation process of the superhydrophobic photothermal oil-absorbing LPUF is shown in Fig. 1a. Through sulfuric acid-catalyzed reactions between solvents and lignin, a black and uniform LLP was produced. This process not only increased the spatial distance between the lignin backbone and hydroxyl groups but also exposed more reactive sites. Additionally, phenolic hydroxyl groups were converted into more reactive aliphatic hydroxyl groups, significantly enhancing the reactivity of LLP in polyurethane synthesis. The hydroxyl content of LLP was determined by 31P NMR. After liquefaction, the phenolic hydroxyl and carboxyl groups in LLP disappeared, while the content of aliphatic hydroxyl groups increased. As shown in Fig. 1b, the chemical shift of water, used as a reference peak, was at 132.20 ppm, and the internal standard cyclohexanol appeared at 145.15 ppm. The peak for aliphatic hydroxyl groups was observed between 150 and 146 ppm, while phenolic hydroxyl groups appeared between 144 and 137 ppm. Table S3† shows that the hydroxyl values of LLP15, LLP22.5, LLP30, and LLP37.5 were 7.9 mmol g^{-1}, 7.3 mmol g^{-1}, 6.9 mmol g^{-1}, and 6.7 mmol g^{-1}, respectively. Since lignin primarily contains phenolic hydroxyl groups, the content of aliphatic hydroxyl groups in the polyols decreased as the lignin content increased.

The viscosity of LLP significantly increased with the addition of more lignin. As shown in Fig. 1c, at 25 °C, the viscosities of LLP15, LLP22.5, LLP30, and LLP37.5 were 1.59 Pa s, 5.76 Pa s, 12.03 Pa s, and 28.44 Pa s, respectively. The viscosity of LLP was highly temperature-sensitive, particularly for LLP37.5, whose viscosity decreased significantly with increasing temperature. Due to the high viscosity of LLP, it was difficult to achieve uniform mixing with HDI. Multiple foaming experiments revealed that polyols with higher viscosities resulted in smaller foam volumes and uneven foam structures. Consequently, LLP37.5 was excluded from subsequent foaming and modification experiments.

The XPS analysis of LPUF30 and LPUF30-2 further revealed the changes in the chemical composition of the materials. In the spectrum of Fig. 1d, the C 1s peak at 286 eV, the O 1s peak at 399 eV, and the N 1s peak at 532 eV indicate the typical chemical composition of the polyurethane foam. In Fig. 1e, the C 1s spectrum of LPUF30 is deconvoluted into four peaks at binding energies of 284.8, 285.4, 286.4, and 289.1 eV, indicating that carbon primarily exists in the forms of C–C, C–N, C–O, and C=O, which are characteristic of polyurethane. As shown in Fig. 1f, the N 1s peak of LPUF30-2 is significantly reduced compared to LPUF30 after ODTMS modification. This reduction is due to the introduction of polysiloxane, which altered the chemical environment on the material's surface, reducing the exposure of nitrogen atoms. Additionally, the appearance of Si 2p and Si 2s peaks in the LPUF30-2 sample indicates the successful incorporation of silicon into the polyurethane matrix, further confirming the effective modification by ODTMS. Fig. 1g shows the Si 2p core-level spectrum of the LPUF30-2 sample, with two distinct peaks at 103.1 eV and 101.8 eV corresponding to the presence of Si–O–Si and Si–O–C bonds, respectively, reflecting

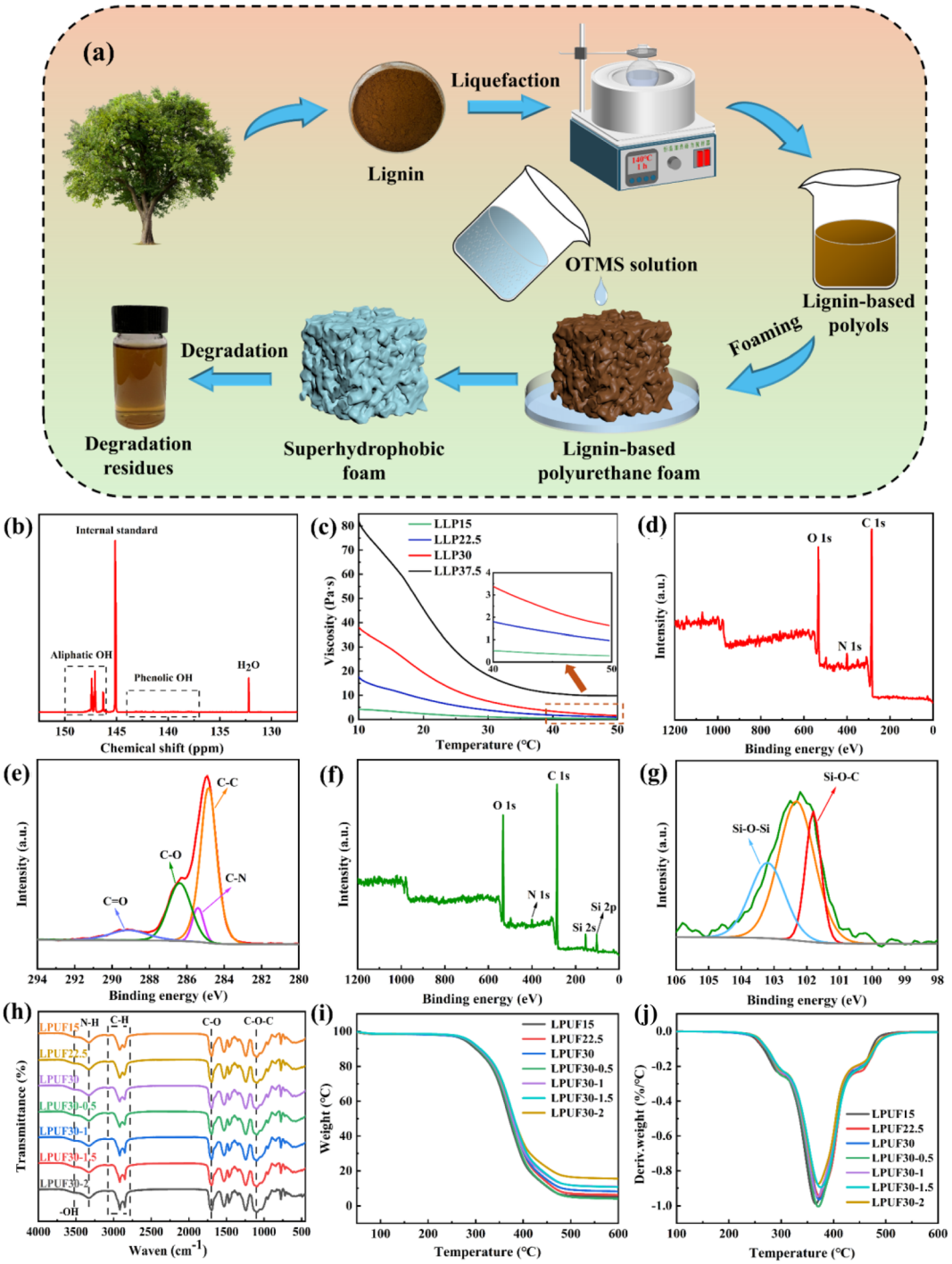

Fig. 1 (a) The schematic diagram of the preparation and degradation of superhydrophobic photothermal oil-absorbing LPUF. (b) 31P NMR spectrum of LLP30. (c) Relationship between viscosity and temperature of polyols LLP15, LLP22.5, LLP30 and LLP37.5 (d) XPS full spectrum of LPUF30. (e) XPS spectrum of LPUF30 in the C 1s region. (f) XPS full spectrum of LPUF30-2. (g) XPS spectrum of LPUF30-2 in the Si 2p region. (h) FT-IR spectra of LPUF15, LPUF22.5, and LPUF30 series samples. (i) TGA curves of LPUF15, LPUF22.5, and LPUF30 series samples. (j) DTG curves of LPUF15, LPUF22.5, and LPUF30 series samples.

the attachment of polysiloxane. The XPS results confirm that long-chain alkyl groups were successfully integrated into the polyurethane matrix, further validating the impact of ODTMS modification on the chemical composition of the foam surface.

The FT-IR spectra of LPUF are shown in Fig. 1h. All LPUF samples exhibited similar FT-IR spectra, indicating that their chemical structures remain consistent in the basic framework. The prominent peaks at 2920 cm^{-1} and 2850 cm^{-1} correspond to the C–H stretching vibrations of CH3 and CH2 groups, confirming the stable presence of alkyl chains in the polyurethane foam. The C–O–C stretching vibration at 1100 cm^{-1} is attributed to polyethylene glycol-400, indicating that the polyether

segment participated in the formation of the foam network structure. The N–H stretching vibration at 3328 cm^{-1} arises from the asymmetric stretching of the urethane bonds. The broad peak at 3525 cm^{-1} is due to the stretching vibration of free –OH groups, indicating the presence of hydroxyl groups on the foam surface. Peaks at 1700 cm^{-1}, 1530 cm^{-1}, and 1240 cm^{-1} correspond to the C=O stretching in urethane, urea, and ether groups, respectively, which are characteristic of polyurethane's inherent structure. The strong C=O peak at 1700 cm^{-1} confirms the formation of amide bonds in the material, indicating a complete reaction between isocyanate and polyol. Furthermore, the disappearance of the NCO peak at 2280 cm^{-1} further proves the complete formation of the polyurethane network structure, with no unreacted groups remaining. These conclusions confirm the successful synthesis of LPUF. After modification with ODTMS, the intensity of the C–H peaks slightly increased, which is attributed to the introduction of long-chain alkyl siloxane structures following the hydrolysis and condensation of ODTMS. The introduction of polysiloxane enhanced the hydrophobicity of the foam surface, as reflected by the increased C–H stretching vibration peaks, indicating the successful attachment of organosilicon to the foam skeleton.

As shown in Fig. 1i and j, the T5% of LPUF15, LPUF30, and LPUF30-2 were 276 °C, 280 °C, and 286 °C, respectively. The first stage, from 250 °C to 350 °C, corresponds to the degradation of urethane bonds and the breaking of ether bonds in lignin. The second stage (between 350 °C and 450 °C) represents the weight loss caused by the decomposition of the polyether segments in the polyurethane. At 600 °C, the residual mass of LPUF30-2 reached 15.50%, which was 7.31% higher than that of LPUF, due to the presence of polysiloxane. The thermogravimetric results indicate that the thermal stability of the foam increased with the ODTMS content.

The SEM images are shown in Fig. 2. Due to the high viscosity of the system, the gas bubbles could not be uniformly dispersed during the foaming process, resulting in the formation of larger pores. As a result, the pore size of LPUF increased slightly with the addition of lignin. Upon magnification, it was observed that the surface of the unmodified foam was smooth, while the surface of the modified foam was covered with layered material, indicating that the polysiloxane produced by the hydrolysis and condensation of ODTMS adhered to the foam skeleton, forming a hydrophobic layer. Additionally, the modified foam exhibited larger pore channels, which are more favorable for the adsorption and storage of oil pollutants. The chemical composition of LPUF30-2 was determined using energy-dispersive spectroscopy (EDS) attached to the SEM. The results confirmed that the foam contained the elements C, N, O, and Si, where C, N, and O originated from the polyurethane foam, and Si was derived from ODTMS.

3.2. Oil adsorption and separation capacity

Water contact angle (WCA) is a critical indicator for evaluating the wetting behavior of materials. Superhydrophobicity is

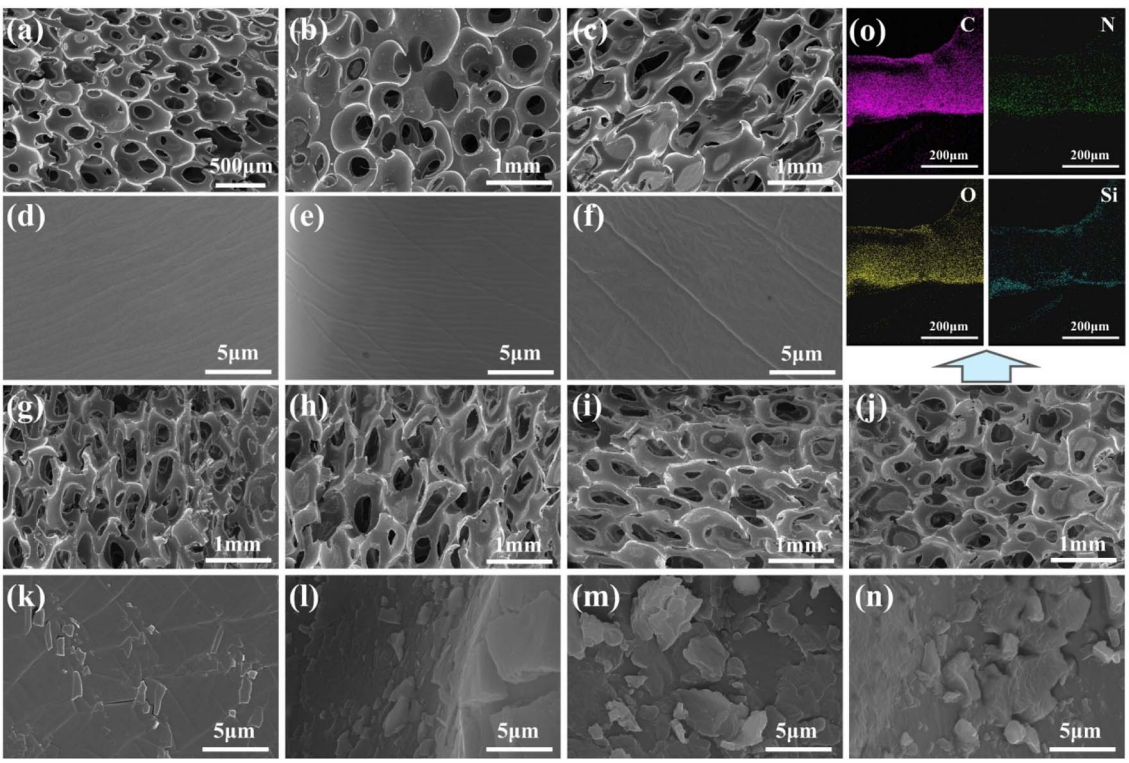

Fig. 2 SEM images of the surface of the prepared foams and magnified images of their skeleton regions: (a and d) LPUF15, (b and e) LPUF22.5, (c and f) LPUF30, (g and k) LPUF30-0.5, (h and l) LPUF30-1, (i and m) LPUF30-1.5, (j and n) LPUF30-2, (o) EDS spectrum of C, N, O, and Si elements in LPUF30-2.

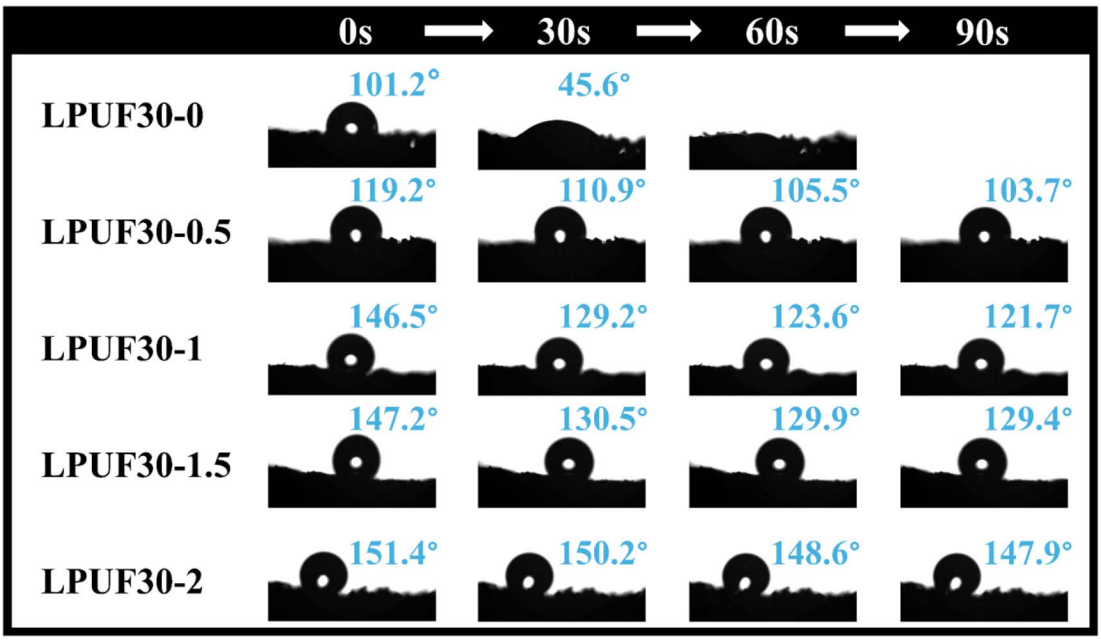

Fig. 3 Water contact angle (WCA) and retention time of LPUF30 series samples.

a necessary condition for adsorbents to achieve high oil–water separation performance, and this property is primarily influenced by the surface energy and surface roughness of the material. As shown in Fig. 3, the WCA of LPUF30-0 is 101.2°, slightly higher than that of commercial polyurethane foam (WCA around 85°). Using an optical camera, it was observed that the water droplet was quickly absorbed by LPUF30-0 after being dropped, and it was fully absorbed within 60 seconds. As the concentration of ODTMS modification increased, the WCA of the foam surface gradually increased, with a significant improvement in hydrophobicity observed in the concentration range from 0.5% to 1%. This is because the long alkyl chains (octadecyl) in ODTMS form a hydrophobic layer on the foam surface, which reduces the surface energy of the foam, making it more difficult for water droplets to wet the surface, thereby significantly enhancing the hydrophobicity of the material. The WCA of LPUF30-2 reached as high as 151.4°, indicating that the sample achieved a superhydrophobic state (WCA > 150°). These results confirm the effectiveness of ODTMS in enhancing the hydrophobicity of LPUF.

LPUF30-2 exhibits excellent three-dimensional pore structure, durability, and superhydrophobicity, enabling it to separate organic solvents and oils from water environments. Toluene and dichloromethane were dyed with Oil Red O to simulate floating oil pollutants on the water surface and submerged oil pollutants, respectively. LPUF30-2 was then used to adsorb these oils in separate tests (Fig. 4). The experimental results showed that the foam exhibited a high selectivity for toluene floating on the water surface, quickly adsorbing it into its porous structure while repelling water (Video S1†). In the underwater environment, LPUF30-2 also demonstrated effective adsorption of dichloromethane deposited in water (Video S2†). Traditional polyurethane foam lacks oil selectivity and a non-polar surface, making it difficult to establish effective interactions with non-polar oil molecules, and thus unable to exhibit significant oil adsorption performance.[47,53] Through modification, lignin-based foam incorporates non-polar groups such as long-chain alkyl groups on its surface, significantly enhancing its affinity for oil molecules. Additionally, this modification effectively reduces the adsorption tendency toward water molecules, enabling lignin-based foam to exhibit higher selectivity in oil–water mixtures and demonstrating excellent oil adsorption performance. These experiments demonstrated the high efficiency of LPUF30-2 in adsorbing oil pollutants across diverse water environments, further establishing its strong potential for extensive applications in oil spill remediation.

A mixture of 100 mL chloroform and water (V : V = 1 : 1) was added to a separator to verify the separation efficiency of LPUF30-2 (Fig. 5a). When the mixture was poured in, chloroform quickly entered the foam's pore structure under gravity and subsequently collected in the receiving flask (Video S3†). Once the chloroform was fully collected, the water solution was blocked by the superhydrophobic foam, preventing it from passing through into the collection flask. These results confirm that LPUF30-2 can easily adsorb oil while blocking water, achieving a high oil–water separation efficiency of up to 97%.

Adsorption capacity is a key metric for evaluating the performance of adsorbents; the higher the adsorption capacity, the more efficient and promising the material is for oil recovery applications. LPUF30-2's actual oil adsorption capacity was investigated using seven common oil pollutants: *n*-hexane, *n*-hexadecane, *n*-octane, toluene, benzene, tetrahydrofuran, and dichloromethane. As shown in Fig. 5b, LPUF30-2 exhibited an adsorption capacity of 4 to 20 times its own weight for these organic solvents. When exposed to an oil-rich environment, the oil was rapidly adsorbed and stored within the foam's three-

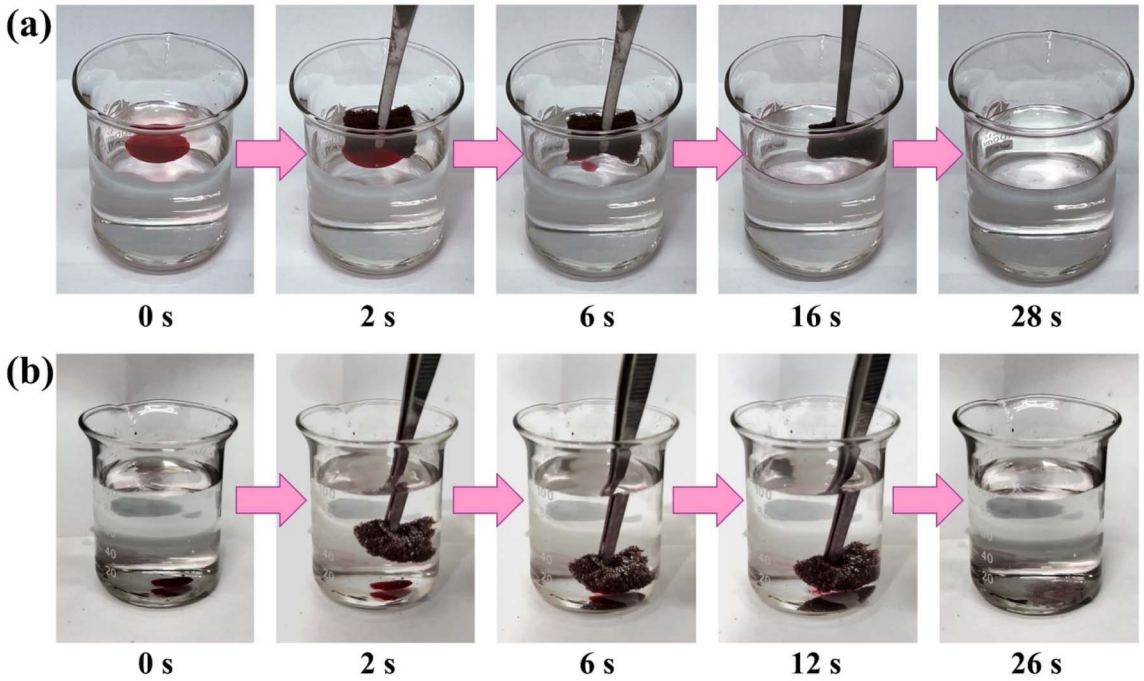

Fig. 4 (a) Adsorption of toluene on the water surface by LPUF30-2. (b) Adsorption of dichloromethane underwater by LPUF30-2 (both toluene and dichloromethane were dyed with Oil Red O).

dimensional pore structure *via* capillary action. The three-dimensional porous structure and large specific surface area of LPUF30-2 allow it to accommodate a greater volume of high-density organic solvents. These structural features enhance capillary adsorption effects and provide ample storage capacity, thereby improving its adsorption capability for high-density solvents. Furthermore, the mass of high-density solvents is greater per unit volume, leading to a positive correlation between the adsorption capacity of LPUF30-2 and the density of organic solvents.

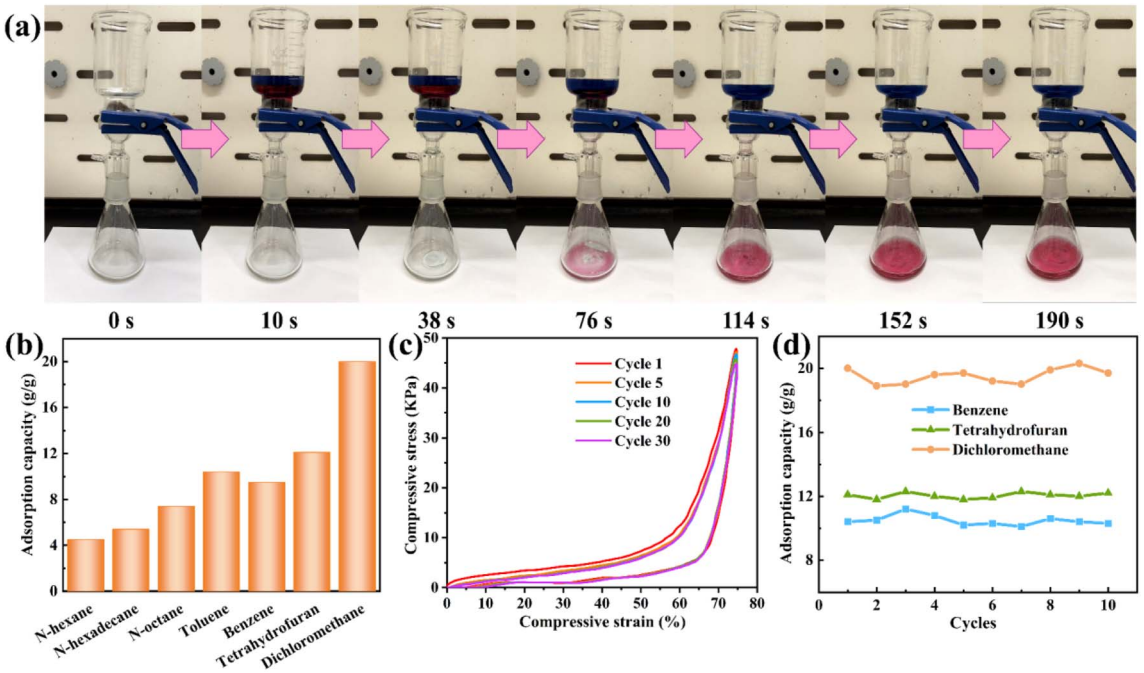

Fig. 5 (a) Separation ability of LPUF30-2 for a chloroform and water mixture (V : V = 1 : 1). (b) Adsorption capacity of LPUF30-2 for different organic solvents. (c) 30-cycle compression curve of LPUF30-2. (d) Cyclic adsorption capacity of LPUF30-2 for different organic solvents.

Excellent structural stability is a prerequisite for superhydrophobic foams to continuously perform oil–water separation, which requires high elastic recovery performance. The cyclic stress–strain curves of LPUF30 and LPUF30-2 under 75% strain are shown in Fig. S1† and 5c. Due to its larger pore structure, LPUF30-2 is softer, with a compressive strength of 47 kPa. After 30 mechanical compression cycles, LPUF30-2 exhibited a maximum compressive stress attenuation rate of only 2.52%, demonstrating excellent elastic recovery ability. In practical applications, high mechanical stability ensures that the foam can maintain its excellent adsorption performance even after multiple adsorption-squeezing cycles. LPUF30-2 showed good adsorption capacity and significant oil absorption performance, indicating its applicability in the separation and adsorption of oil–water mixtures. Moreover, the reusability of adsorbents is a key factor in determining their practicality. To further investigate the cyclic adsorption capacity of LPUF30-2 for various oil pollutants, benzene, tetrahydrofuran, and dichloromethane were used to evaluate its reusability (Fig. 5d). After 10 adsorption cycles, the adsorption capacity of LPUF30-2 remained almost unchanged, demonstrating its excellent reusability.

3.3. Photothermal oil absorption performance

Crude oil exhibits high viscosity at room temperature, which leads to slower adsorption rates when using conventional adsorbents for oil recovery. This is the primary challenge faced when applying adsorbents for crude oil recovery. Under visible or near-infrared light irradiation, the conjugated structure and molecular stacking of lignin lower the electron transition barrier, promoting the transition of electrons from low-energy orbitals to high-energy orbitals, thereby generating a photothermal effect. [54] Additionally, LPUF, similar to enzymatic hydrolysis lignin, has a dark brown color, which gives it a high light absorption rate and further enhances its photothermal conversion efficiency. As shown in Fig. 6a, under simulated sunlight irradiation with an intensity of 1 kW m^{-2}, the surface temperature of LPUF30-2 reached 76 °C after 300 s, indicating excellent photothermal conversion capability. To demonstrate the practical benefits of LPUF30-2's photothermal conversion for oil spill adsorption, block-shaped LPUF30-2 was placed on the surface of crude oil floating on water to conduct adsorption experiments (Fig. 6b and Video S4†). Multiple adsorption–desorption cycles of crude oil were performed using LPUF30-2. As shown in Fig. 6c, the saturation adsorption capacity of LPUF30-2 for crude oil was approximately 8.1 g g^{-1}. After the first cycle, some crude oil remained attached to the foam's pore structure and could not be completely squeezed out manually, leading to lower adsorption capacities during the second and third cycles, but the capacity stabilized afterward. These results demonstrate that LPUF30-2 exhibits highly efficient photothermal conversion and can achieve effective adsorption and recovery of spilled crude oil in aquatic environments.

The surface of LPUF30-2 exhibits a certain degree of self-cleaning ability in aqueous environments. As shown in Fig. S2,† when sand and soil particles adhered to the surface of

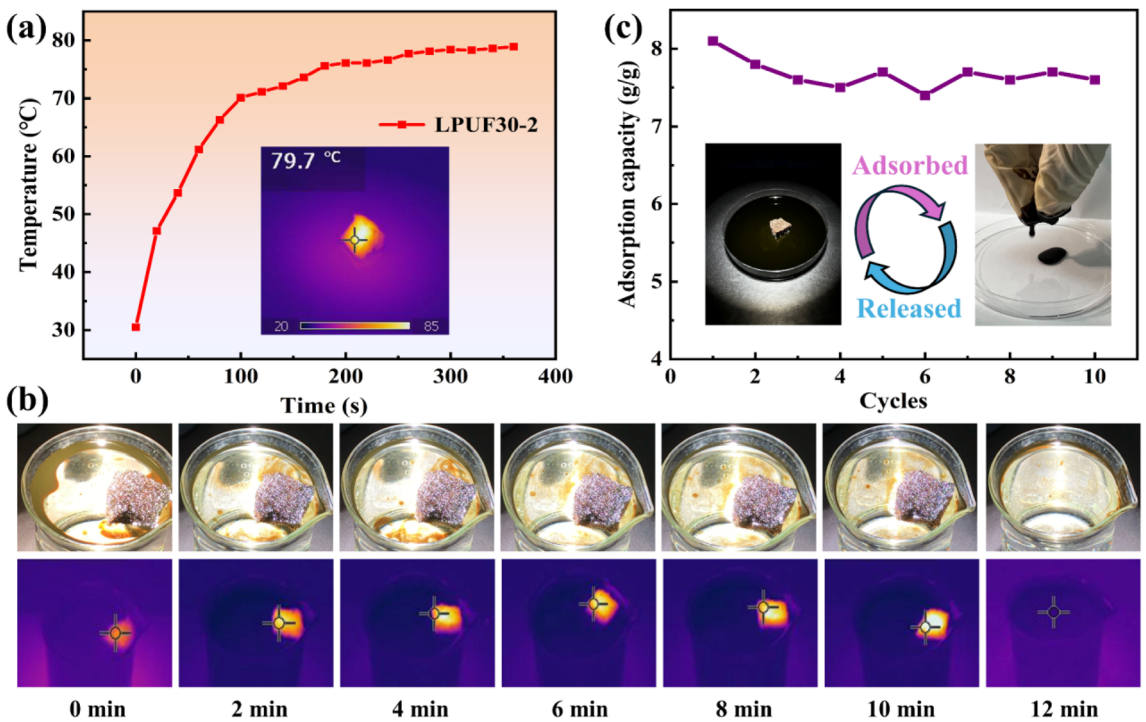

Fig. 6 (a) The maximum surface temperature of LPUF30-2 as a function of time. Inset: 2D infrared image of the LPUF30-2 sample under simulated sunlight radiation. (b) Photos of the crude oil adsorption process by LPUF30-2 under simulated sunlight, along with corresponding 2D infrared images. (c) Cyclic adsorption capacity of LPUF30-2 for crude oil. Inset: adsorption and manual squeezing desorption of the foam adsorbent.

LPUF30-2 foam, these particles were easily carried away by water droplets from the superhydrophobic surface. After the water droplets flowed over the surface, LPUF30-2 became gradually cleaner, with only a few small particle deposits entering the surface pores. To investigate the degradation properties of LPUF, a degradation experiment was conducted on LPUF30-2. Initially, a block of LPUF30-2, with dimensions of 5 mm × 5 mm × 10 mm, was soaked in deionized water at 60 °C. After several hours, no noticeable changes in shape or structure were observed, and the mass loss was negligible upon measurement. The same-sized LPUF30-2 block was then placed in a methanol-0.2 mol L^{-1} sodium hydroxide aqueous solution (V : V = 1 : 1) and its degradation behavior was monitored in a 60 °C water bath. As shown in Fig. S3,† after 5 hours, the foam solid in the sample vial had completely disappeared, and the solution had turned from colorless to dark brown. No solid residue was recovered after vacuum filtration of the mixture in the vial, indicating that the foam material had fully depolymerized, with a degradation rate of 100%. The complete degradation of the foam occurred because the ether bonds in lignin were attacked by hydroxide ions under alkaline conditions, leading to hydrolysis and cleavage, which subsequently caused the entire LPUF to depolymerize into smaller monomers.

4. Conclusions

In this study, LPUF was first prepared using a one-pot method, followed by modification with ODTMS to impart superhydrophobicity. We systematically investigated the effects of lignin content and ODTMS concentration on the microstructure and properties of LPUF. Finally, we explored the adsorption performance of LPUF adsorbents for crude oil and various organic solvents, validating its potential application in water-based oil spill adsorption. The modified LPUF30-2 exhibited excellent elastic recovery performance, good thermal stability, and remarkable oil–water separation capabilities. After 30 cycles of compression, the maximum compression stress decay rate of the foam was 2.52%, demonstrating good elastic recovery. In adsorption tests for crude oil and organic solvents, LPUF30-2 showed a high adsorption capacity, with adsorption capacities of 8.1 g g^{-1} for crude oil and 20 g g^{-1} for dichloromethane, and its adsorption performance remained largely unchanged after 10 adsorption–desorption cycles. Additionally, LPUF30-2 displayed excellent photothermal conversion properties, reaching a surface temperature of 76 °C after 300 s of solar irradiation. The photothermal conversion effect of LPUF under light increased the surface temperature, significantly reducing the viscosity of crude oil, thus accelerating its penetration into the porous structure. The used foam adsorbent, when placed in a methanol-0.2 mol L^{-1} sodium hydroxide aqueous solution (V : V = 1 : 1) and treated at 60 °C for 5 hours, achieved a degradation rate of 100%. The superhydrophobic LPUF developed in this study is a high-performance, environmentally friendly polyurethane foam adsorbent, with the potential to address the shortcomings of traditional petroleum-based polyurethane. It also offers new insights into the high-value utilization of lignin. Crude enzymatic hydrolysis lignin is generally cheaper than petroleum-based polyols, offering potential for cost reduction in polyurethane foam production. However, current industrial-scale production remains costly. Future research will focus on reducing energy consumption during manufacturing to lower costs and enhance application potential. Detailed cost analysis and scalability assessments will further evaluate its economic feasibility. The environmentally friendly adsorbent developed in this study can adsorb and remove oil pollutants from water environments, providing new avenues for oil spill treatment, with promising application potential.

Data availability

The data supporting this study's findings are available from the corresponding author upon reasonable request.

Author contributions

Xinglin Li: writing – review & editing, writing – original draft, visualization, validation, investigation, formal analysis, data curation. Jing Zhang: software, methodology, conceptualization. Hong Liu: software. Zhiyu Li: validation, resources, supervision, meth-odology, conceptualization. Guanfeng Zheng: validation, software. Ling Zhou: supervision, methodology. Peng Fu: validation, software, resources, project administration, methodology, investigation, funding acquisition, conceptualization.

Conflicts of interest

There are no conflicts to declare.

Acknowledgements

This work was supported by the National Natural Science Foundation of China (no. 52376199), the Special Project Fund of "Taishan Scholar" of Shandong Province (no. tsqn202103066), the Youth Innovation Support Program of Shandong Colleges and Universities (2023KJ333).

References

1 P. Sanghamitra, D. Mazumder and S. Mukherjee, *J. Environ. Sci. Health, Part A: Toxic/Hazard. Subst. Environ. Eng.*, 2021, **56**, 394–412.
2 Z. Guo, B. Long, S. Gao, J. Luo, L. Wang, X. Huang, D. Wang, H. Xue and J. Gao, *J. Hazard. Mater.*, 2021, **402**, 123838.
3 J. Li, Y. Wang, R. Gao, T. C. Zhang and S. Yuan, *J. Environ. Chem. Eng.*, 2022, **10**, 107618.
4 W. Zhou, B. Zhan, Z. Chen, G. Wang and Y. Liu, *Sep. Purif. Technol.*, 2023, **320**, 124117.
5 Y. Wang, S. Zhao, Z. Guo, J. Huang and W. Liu, *Colloids Surf., A*, 2021, **628**, 127299.
6 Y. Zhang, J. Liu, L. Ouyang, J. Li, G. Xie, Y. Yan and C. Weng, *Langmuir*, 2021, **37**, 7043–7054.

7 L. Álvarez-Gil, J. Ramírez and P. Fernández-Morales, *Surf. Interfaces*, 2021, **26**, 101362.
8 J. Liang, S. Lin, X. Feng and Q. Pan, *J. Porous Mater.*, 2023, **30**, 1937–1951.
9 Y. Kong, S. Zhang, Y. Gao, X. Cheng, W. Kong, Y. Qi, S. Wang, F. Yin, Z. Dai, Q. Yue and B. Gao, *J. Hazard. Mater.*, 2022, **423**, 127064.
10 S. Deng, C. Zhao, L. Zhu, H. Huang, Y. Li, D. Xiang, H. Li, Y. Wu and S. Huang, *J. Appl. Polym. Sci.*, 2021, **139**, 51521.
11 T. R. B. Tomon, C. J. M. Omisol, B. J. M. Aguinid, K. X. L. Sabulbero, A. C. Alguno, R. M. Malaluan and A. A. Lubguban, *Sci. Rep.*, 2024, **14**, 14223.
12 A. B. Olabintan and T. A. Saleh, *React. Funct. Polym.*, 2024, **195**, 105807.
13 C. M. Yu, X. H. Zhuang, S. W. Zeng, Q. X. Dong, Z. X. Jing, P. Z. Hong and Y. Li, *RSC Adv.*, 2019, **9**, 17543–17550.
14 L. Zeng, F. Wang, S. Han, M. Li, S. Tu, Q. Lu and W. Cao, *J. Am. Ceram. Soc.*, 2021, **104**, 5529–5536.
15 M. R. Sabouri, V. Javanbakht, D. J. Ghotbabadi and M. Mehravar, *Process Saf. Environ. Prot.*, 2019, **126**, 182–192.
16 Z. Li, Q. Tian, J. Xu, S. Sun, Y. Cheng, F. Qiu and T. Zhang, *ACS Appl. Mater. Interfaces*, 2021, **13**, 51652–51660.
17 M. H. Tran and E. Y. Lee, *Environ. Chem. Lett.*, 2023, **21**, 2199–2223.
18 Z. Huang, H. Wang, J. Du, X. Liu, G. Pan, X. Yin, W. Lin, X. Lin, Y. Sun, G. Yi and L. Niu, *Chem. Eng. J.*, 2023, **473**, 145423.
19 S. Kim, K. Li, A. Alsbaiee, J. P. Brutman and W. R. Dichtel, *Adv. Mater.*, 2023, **35**, e2305387.
20 H. Zhao, W. C. Gao, Q. Li, M. R. Khan, G. H. Hu, Y. Liu, W. Wu, C. X. Huang and R. K. Y. Li, *Adv. Colloid Interface Sci.*, 2022, **303**, 102644.
21 X. Li, Y. Bi and G. Bi, A comparative study of polyurethane foam by substituting LBA using green polyurethane foam CFA-1, *J. Appl. Polym. Sci.*, 2024, **141**(14), e55177.
22 J. Wang, C. Zhang, Y. Deng and P. Zhang, *Polymers*, 2022, **14**, 4586.
23 S. Mallakpour and V. Behranvand, *J. Cleaner Prod.*, 2021, **312**, 127513.
24 P. H. Hoang, H. T. Dat, T. D. Cuong and L. Q. Dien, *RSC Adv.*, 2022, **12**, 14976–14985.
25 A. Sittinun, P. Pisitsak and S. Ummartyotin, *Compos. Commun.*, 2020, **20**, 100351.
26 G. Zhu, X. Li and X. Zhang, *Colloids Surf., A*, 2024, **681**, 132811.
27 J. Wang, H. Wang, Y. Wang, P. Gao, F. Wang, X. Men, Z. Zhang and Y. Lu, *Chem. Eng. J.*, 2021, **420**, 129806.
28 M. Zaman Khan, J. Militky, M. Petru, B. Tomková, A. Ali, E. Tören and S. Perveen, *Eur. Polym. J.*, 2022, **178**, 111481.
29 W. Kong, K. Yang, Y. Chen, W. Shao, C. Jia, J. Zhu and J. He, *Prog. Org. Coat.*, 2025, **198**, 108934.
30 L. He, X. Qi, W. Wei, X. Zhang, J. Wang and Z. Gao, *J. Hazard. Mater.*, 2024, **477**, 135222.
31 M. V. G. Zimmermann, A. J. Zattera, B. R. Fenner and R. M. C. Santana, *Polym. Bull.*, 2020, **78**, 1423–1440.
32 D. Yuan, T. Zhang, Q. Guo, F. Qiu, D. Yang and Z. Ou, *Chem. Eng. J.*, 2017, **327**, 539–547.
33 X. Ma, J. Chen, J. Zhu and N. Yan, *Macromol. Rapid Commun.*, 2021, **42**, e2000492.
34 S. Li, Y. Zhang, X. Ma, S. Qiu, J. Chen, G. Lu, Z. Jia, J. Zhu, Q. Yang, J. Chen and Y. Wei, *Biomacromolecules*, 2022, **23**, 1622–1632.
35 Y. Ma, Y. Xiao, Y. Zhao, Y. Bei, L. Hu, Y. Zhou and P. Jia, *React. Funct. Polym.*, 2022, **175**, 105285.
36 D. Dukarska and R. Mirski, *J. Compos. Sci.*, 2024, **8**, 286.
37 J. Du, H. Wang, Z. Huang, X. Liu, X. Yin, J. Wu, W. Lin, X. Lin and G. Yi, *Int. J. Biol. Macromol.*, 2023, **248**, 125925.
38 J. Deng, S.-F. Sun, E.-Q. Zhu, J. Yang, H.-Y. Yang, D.-W. Wang, M.-G. Ma and Z.-J. Shi, *Ind. Crops Prod.*, 2021, **164**, 113412.
39 T. R. Araujo, D. Bresolin, D. de Oliveira, C. Sayer, P. H. H. de Araújo and J. V. de Oliveira, *Eur. Polym. J.*, 2023, **188**, 111934.
40 H. Li, Y. Liang, P. Li and C. He, *J. Bioresour. Bioprod.*, 2020, **5**, 163–179.
41 N. Sun, M. Di and Y. Liu, *Int. J. Biol. Macromol.*, 2021, **184**, 1–8.
42 Y. Wang, H. Wang, Z. Li, D. Yang, X. Qiu, Y. Liu, M. Yan and Q. Li, *J. Colloid Interface Sci.*, 2021, **594**, 316–325.
43 X. Ma, S. Li, F. Wang, J. Wu, Y. Chao, X. Chen, P. Chen, J. Zhu, N. Yan and J. Chen, *ChemSusChem*, 2023, **16**, e202202071.
44 L. Wu, S. Liu, Q. Wang, Y. Wang, X. Ji, G. Yang, J. Chen, C. Li and P. Fatehi, *Ind. Crops Prod.*, 2022, **177**, 114526.
45 C. Li, H. Jin, M. Hou, X. Guo, T. Xiao, X. Cao, W. Jia, P. Fatehi and H. Shi, *Int. J. Biol. Macromol.*, 2023, **256**, 128290.
46 X. Ma, C. Zhang, P. Gnanasekar, P. Xiao, Q. Luo, S. Li, D. Qin, T. Chen, J. Chen, J. Zhu and N. Yan, *Chem. Eng. J.*, 2021, **415**, 128956.
47 J. Wu, X. Ma, P. Gnanasekar, F. Wang, J. Zhu, N. Yan and J. Chen, *Sci. Total Environ.*, 2023, **860**, 160276.
48 E. I. Evstigneyev and S. M. Shevchenko, *Wood Sci. Technol.*, 2020, **54**, 787–820.
49 J. Chen, J. Wu, Y. Zhong, X. Ma, W. Lv, H. Zhao, J. Zhu and N. Yan, *Sep. Purif. Technol.*, 2023, **311**, 123284.
50 J. Huang, H. Wang, W. Liu, J. Huang, D. Yang, X. Qiu, L. Zhao, F. Hu and Y. Feng, *Int. J. Biol. Macromol.*, 2023, **225**, 1505–1516.
51 S. Rath, D. Pradhan, H. Du, S. Mohapatra and H. Thatoi, *Adv. Compos. Hybrid Mater.*, 2024, **7**, 27.
52 J. Hu, M. Huang, X. Zhou, R. Luo, L. Li and X. Li, *Polymers*, 2024, **16**, 2340.
53 R. Mohammadpour and G. Mir Mohamad Sadeghi, *J. Polym. Environ.*, 2020, **28**, 892–905.
54 J. Li, W. Liu, X. Qiu, X. Zhao, Z. Chen, M. Yan, Z. Fang, Z. Li, Z. Tu and J. Huang, *Green Chem.*, 2022, **24**, 823.